




Evaluating statistical significance for massive black hole binary mergers with space-based gravitational wave detectors

Hong-Yu Chen(陈洪昱)¹, En-Kun Li(李恩坤)¹, and Yi-Ming Hu(胡一鸣)^{1,*}

¹MOE Key Laboratory of TianQin Mission, TianQin Research Center

for Gravitational Physics & School of Physics and Astronomy,

Frontiers Science Center for TianQin, Gravitational Wave Research Center of CNSA,

Sun Yat-sen University (Zhuhai Campus), Zhuhai, 519082, China

(Dated: May 15, 2025)

Important scientific discoveries should be backed by high statistical significance. In the 2030s, multiple space-based gravitational wave detectors are expected to operate. While many works aim to achieve quick and reliable detection and parameter estimation of millihertz gravitational wave sources, dedicated studies are lacking to assess the significance of space-based detectors. In this work, we propose a framework to assess the statistical significance of massive black hole binaries (MBHBs) detections with space-based gravitational wave detectors. We apply this algorithm to simulated data with Gaussian stationary noise and the complex LDC-2a dataset to measure the false alarm rate and significance of MBHB signals. We also analyze factors affecting the significance of MBHBs and design a method to mitigate multi-source confusion interference. In Gaussian noise conditions, MBHBs with a signal-to-noise ratio of about 7 can achieve 3σ significance, and those with a signal-to-noise ratio of about 8 achieve 4σ . Our analysis demonstrates that all MBHB signals in the LDC-2a dataset have a significance exceeding 4.62σ .

I. INTRODUCTION

Scientific discoveries should be statistically confirmed. When asserting a signal's existence, the null hypothesis probability (the likelihood of obtaining the data if no signal is present) must stay below a predetermined threshold. The discovery threshold is commonly set at 5σ , which corresponds to the probability of a value being 5 or more standard deviations from the mean of a Gaussian distribution [1].

Recent years have seen significant advancements in the field of gravitational wave (GW) astronomy, with nearly a hundred GW events claimed by ground-based GW detectors [2–4]. Subsequently, pulsar timing arrays (PTAs) have also contributed to the field by detecting the background of GWs [5–8]. In the 2030s, space-based GW detectors are expected to further revolutionize this research area [9–12]. Operating in space and covering a lower frequency spectrum, these detectors will likely enhance our understanding of the cosmos.

One of the preliminary sources of space-based GW detectors is massive black hole binary (MBHB) [13, 14]. The space-based GW detectors are expected to observe the MBHB events with redshift up to $z \sim 20$. Detecting GWs from MBHB mergers will be a significant breakthrough in astronomy and cosmology. It will enable unprecedented tests of the theory of general relativity [15–18], offer valuable insights into black hole formation and evolution [19, 20], and provide important information about the universe's expansion [21–24]. With so many important scientific applications deeply tied to the detection, the stakes are too high for us not to be extremely

confident that the detections are genuine. Thus, providing a reliable assessment of the significance and false alarm rate (FAR) of MBHB signals is crucial for their application in astronomical and fundamental physics research.

Ground-based GW detectors have developed various methods for evaluating significance, including the time-shift method [25] and the Poisson estimation method [26]. However, no research team has yet explored significance evaluation methods for space-based GW detectors. Space-based detectors' unique data characteristics complicate this process. In the millihertz frequency band, GW signals exhibit longer durations, causing multi-source confusion [27–29]. The satellite's orbit around its geometric center as well as the Sun creates a complex time-varying response, increasing the time and effort required to model the signals [30–32]. Meanwhile, for signals with generally high signal-to-noise ratio (SNR), more details like higher harmonics are no longer negligible, adding complexities [33]. These factors complicate data analysis for space-based GW detectors and necessitate the development of new methods. Various methodologies have been developed to address the challenges of high-dimensional parameters and multi-source confusion in space-based GW detection, such as wavelet denoising [34], block-Gibbs [35], novel maximum likelihood estimate [36], Reversible Jump Monte-Carlo Markov chains [29, 37, 38], and near real-time analysis [39]. However, none of them have identified the signals they found or studied their FAR and significance.

This work aims to develop a significance evaluation algorithm suitable for space-based GW detectors, specifically for the detection of MBHB mergers. In this study, we will select suitable time-shift intervals for space-based GW detectors and construct a significance evaluation pipeline based on the iterative Nelder-Mead algorithm.

* huyiming@sysu.edu.cn

In addition, we will apply our algorithm to both Gaussian stationary noise and the more realistic LDC-2a dataset [40]. The latter presents multi-source confusion from numerous Galactic binaries (GBs) and MBHBs. We will analyze how foreground noise and multi-source confusion affect the significance of MBHBs. This analysis can offer insights for future advanced ground-based GW detectors, which may also face this issue.

This paper is organized as follows: Section II gives an overview of the theoretical background of significance and its evaluation. In Section III, we analyze both the simulated Gaussian noise data and the LDC-2a Sangria dataset separately. Finally, Section IV summarizes the entire work. Appendix A provides a brief introduction to future space-based GW detectors. Appendix B presents the MBHB waveforms used in this work.

II. THEORETICAL BACKGROUND

A. Statistical significance

Significance quantifies the likelihood that an observed result is genuine rather than a random fluctuation. When the false alarm probability (FAP) is below the probability corresponding to several standard deviations away from the mean of a Gaussian distribution, the significance of the signal is quantified using this σ value, as shown in Table I.

TABLE I. The relationship between the FAP and significance.

Significance	FAP
1σ	1/6.30
2σ	1/43.9
3σ	1/741
4σ	$1/(3.16 \times 10^4)$
5σ	$1/(3.49 \times 10^6)$

Achieving such high precision FAP is challenging. The time-shift method effectively addresses this by offsetting the two detectors' timestamps to decorrelate the data and construct long-duration equivalent background data. For ground-based detector networks, using this method with several days of observational data from three detectors allows for constructing background data spanning longer than the universe's age [41]. Then, FAR and FAP can be easily calculated by searching for coincident triggers in the equivalent background data:

$$\text{FAR} = \frac{N_{\text{FA}}}{T_{\text{tot}}}, \quad (1)$$

$$\text{FAP} = \frac{T_{\text{obs}} \times N_{\text{FA}}}{T_{\text{tot}}}, \quad (2)$$

where N_{FA} indicates the number of coincident triggers in the equivalent background data, T_{tot} and T_{obs} are the total time of equivalent background data and the actual observation time.

B. Assessment of significance

For space-based GW detectors, we can adapt the time-shift concept with targeted optimizations, as depicted in 1. Unlike ground-based detectors that require multiple detectors for time-shifting, a triangular-shaped space-based GW detector includes three interferometers. These data streams can be rearranged into three noise-uncorrelated channels: A , E , and T (see Equation B1). Due to the T channel's low sensitivity, which barely affects the time-shift algorithm's results, we focus on A and E . After whitening, we can construct equivalent background noise from the A and E channels. Considering the light-second scale of space-based detectors, as well as the timing errors, we've chosen a 1-minute interval for time-shifting. This choice is a compromise so that the two data channels are uncorrelated after the time-shift, meanwhile, one can construct large enough background noise.

Time-shift algorithms in ground-based GW detectors contain two assumptions: inclusive background and exclusive background. The latter excludes all triggers with candidates that have a FAR below a specified threshold, thus offering a more conservative description of the noise background distribution [42, 43]. For space-based GW detectors, MBHB signals, due to higher SNRs and longer durations, have a more significant impact on the background distribution. Consequently, this study focuses solely on analyzing the exclusive background from which MBHB signals have been removed.

When identifying triggers in time-shifted data, we used the Nelder-Mead algorithm instead of the traditional template bank method. The latter is computationally impractical for higher-dimensional, longer-duration signals from space-based GW detectors [44, 45]. In contrast, the Nelder-Mead algorithm, a derivative-free multidimensional optimization method [46, 47], exceeds most search algorithms in performance. It needs minimal function evaluations per iteration, usually one or two, making it ideal for resource-heavy function evaluations [48]. Its efficiency and ability to handle non-smooth or discontinuous functions without derivative information make it a suitable choice for fast optimization in practical applications. Though sometimes trapped in local rather than global maxima, iterative algorithms can still identify all posterior probability peaks in data.

In the selection of the detection statistic, we chose an SNR form based on the log-likelihood ratio.

$$\rho = \begin{cases} \sqrt{2 \times \ln \Lambda}, & \Lambda > 0 \\ 0, & \Lambda \leq 0 \end{cases} \quad (3)$$

$$\ln \Lambda = \langle d | h \rangle - \frac{1}{2} \langle h | h \rangle, \quad (4)$$

where, d is the data, and h is the signal template. This form of SNR is better at suppressing triggers caused by noise compared to the optimal SNR in data analysis [49]. For the construction of waveform h , see Appendix B.

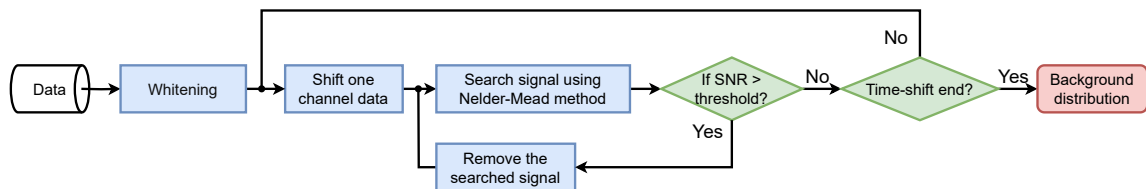


FIG. 1. The significance evaluation pipeline for MBHBs in space-based GW detectors.

After each search, the corresponding signals will be subtracted from the data. The search is then repeated until no MBHB triggers above the threshold are found. By periodically time-shifting the channel data and conducting searches with the Nelder-Mead algorithm after each shift, we can obtain the background distribution of the false alarms. In our algorithm, we allocate the analysis of time-shifted data across varying time intervals to different cores, enabling high parallelism in code execution.

III. RESULT

A. Gaussian Noise

First, we consider the simplest scenario, where the data contains only Gaussian and stationary noise, representing the exclusive background for a single MBHB source during observation. We generated 1 month of Gaussian instrumental noise for TianQin and LISA using the theoretical noise power spectral density (PSD) [32, 50], as shown in Fig. 2(a). Notably, due to LISA's superior low-frequency performance, it is more affected by the GB foreground. Therefore, we also assessed the situation where LISA is impacted by the GB foreground. For simplicity, we consider the stationary GB foreground here. In the next section, we will explore the more realistic impact of GB.

By shifting 1-month observational data at 1-minute intervals, we moved the data 43,200 times to create equivalent background data spanning 3,600 years. For each piece of data, by applying the Nelder-Mead algorithm, we can identify the trigger with the highest SNR within the 1-month period. All triggers with SNR greater than 3 are accumulated and their distribution shown in Fig. 2(b). Since no authentic signals are expected in the time-shifted background, all the triggers can be treated as false alarms. By setting an SNR threshold, one can obtain the FAR as the cumulative count rate of the false alarms which are associated with SNR larger than the threshold. Based on Table I, we calculated the relationship between FAR and significance for a 1-month observation. The lowest FAR of $1/3600 \text{ yr}^{-1}$ corresponds to a significance level of 4.07σ . In Fig. 2(b), we mark the cumulative count rate and significance for MBHB signals with different SNRs.

Based on the SNR distribution of false alarms from Gaussian noise, Table II presents the SNR required for TianQin and LISA (both the instrumental noise itself and that includes foreground noise) to reach 3σ and 4σ . TianQin has a lower FAP for MBHB detection. For LISA, the FAP slightly increases when foreground noise is included.

TABLE II. The SNR required for MBHBs to reach a specified significance level under Gaussian noise for different detectors, assuming a 1-month observation.

Detector	$\rho_0^{3\sigma}$	$\rho_0^{4\sigma}$
TianQin	6.26	7.15
LISA	6.72	7.91
LISA _{foreground}	6.88	7.92

To explore the causes of false alarms and detector-specific FAP differences, we collected false alarms with $\rho \geq 3$. These false alarms are mostly uniformly and randomly distributed in the parameter space but show patterns in chirp mass and luminosity distance. As shown in Fig. 3, most false alarms involve higher or lower masses and greater distances. Luminosity distance affects GW amplitude, while chirp mass determines GW frequency. Since the data are Gaussian noise based on detector PSD, in frequency bands with low PSD, noise and random fluctuations are minimal, leading to weak false-alarm triggers and a low FAP. Consequently, TianQin and LISA have extremely low FAPs in their sensitive bands (corresponding to MBHBs with chirp masses about $\sim 10^5 M_\odot$ and $\sim 10^6 M_\odot$). In contrast, in bands with higher noise PSD, their FAPs are higher. Meanwhile, TianQin's superior sensitivity in higher frequencies gives it a low FAP at the low-mass end. As for the high-mass end, the 10^{-4} Hz truncation of TianQin hinders false alarms from accumulating enough SNR, also keeping the FAP low. For LISA, when considering the foreground, many false alarms appear with a chirp mass of about $10^6 M_\odot$. This corresponds to the noise PSD increase in LISA due to foreground noise at around 1 mHz.

When analyzing Gaussian noise with an SNR threshold of 3 for TianQin, the entire process required approximately 111 hours using 56 cores of an Intel Xeon Gold 6330 CPU. For LISA cases with and without foregrounds, using the same CPU, the computational time was approximately 142 hours and 214 hours, respectively.

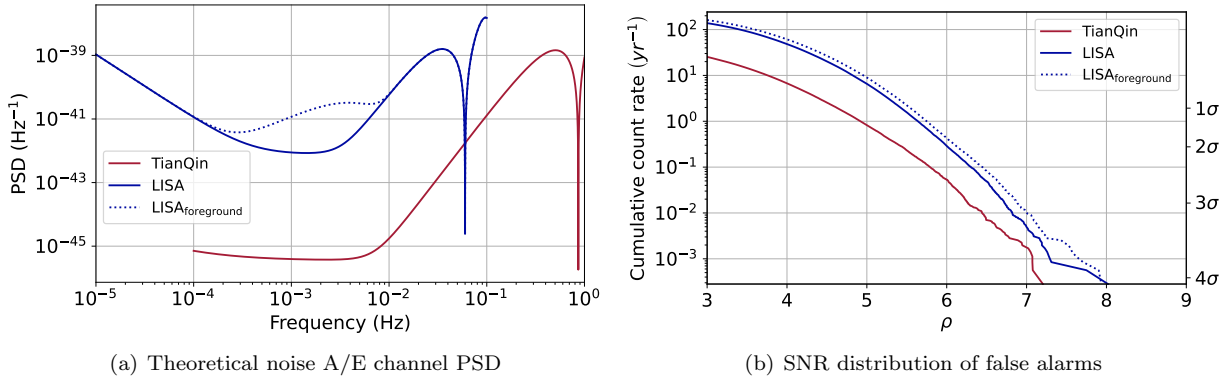


FIG. 2. The left panel shows the theoretical noise A/E channel PSD of TianQin (red) and LISA (blue). The right panel illustrates the SNR distribution of false alarms. The left-hand axis of the right panel shows the cumulative count rate (FAR) at different SNRs. The right-hand axis is the significance corresponding to different FARs. The case for LISA with the foreground is marked with the blue dashed line.

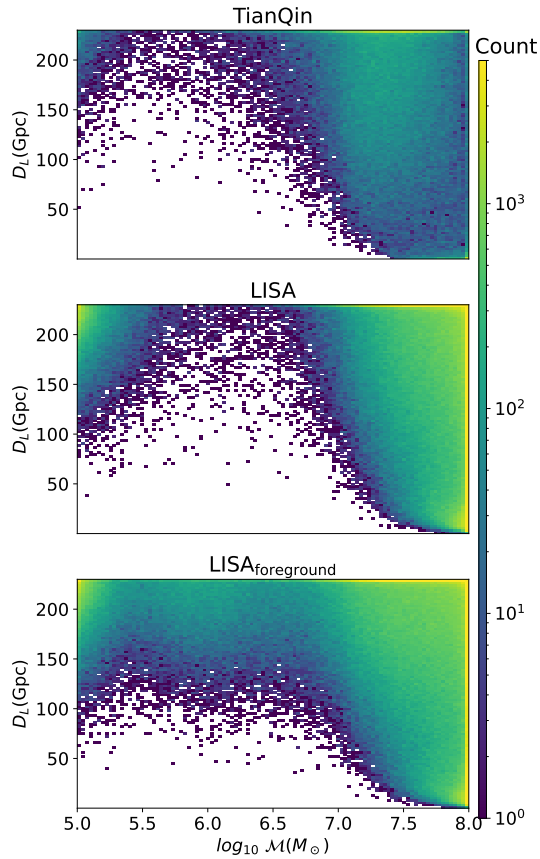


FIG. 3. The histograms of the distribution of false alarms with $\rho \geq 3$ in terms of chirp mass and luminosity distance for different detectors.

B. LDC-2a Sangria Dataset

We then consider a more realistic scenario, analyzing the significance of MBHB signals within the LDC-2a Sangria dataset. This dataset, spanning one year, includes

Gaussian noise, 15 MBHB signals, and approximately 30 million GB signals.

In this analysis, we drop the assumption of the known PSD. So the first step would be estimating the PSD from the Sangria dataset. Cornish [34] proposed methods to estimate two types of PSD for the Sangria dataset: the Spectrum PSD and the Smooth PSD. The Spectrum PSD treats GB signals as non-Gaussian, non-stationary noise and includes their spectral lines in the PSD, facilitating the removal of GB interference during whitening. Conversely, the Smooth PSD offers a PSD without GB spectral lines. We used both PSDs to whiten the Sangria dataset and compared the outcomes.

To reduce contamination from detected signals, we obtained the MBHB parameters in the Sangria dataset via low-latency detection from Cornish [34]. Figure 4 shows the 15 detected signals, with the x-axis representing the SNR under the Smooth PSD, the y-axis showing the relative deviation of SNR, $\Delta\rho/\rho(\text{Smooth PSD})$, and the color indicating the chirp mass. Only one signal has an SNR deviation exceeding 10% in the two PSD conditions. After subtracting these signals from the original dataset, we analyzed the residuals. By conducting 525,600 time-shifts, we generated hundreds of thousands of years of equivalent background data. The lowest FAR of $1/525,600 \text{ yr}^{-1}$ corresponds to a significance level of 4.62σ .

As shown in Fig. 5 and Table III, the significance-to-SNR relationship differs greatly between the two PSDs. In the case of Spectrum PSD, MBHB achieves a 4σ significance at an SNR of about 10, while for Smooth PSD, it requires an SNR near 35. This reveals that the Spectrum PSD significantly suppresses false alarm SNR, thus greatly boosting MBHB significance. This method may apply to other multi-source confusion scenarios. Fortunately, as most MBHBs have large SNR, after hundreds of thousands of time-shifts, no false alarm reaches the SNR level of detected signals. Thus, we can confidently state that all 15 signals have a significance level exceeding

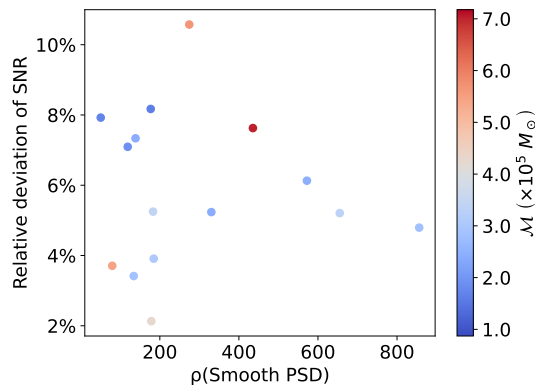


FIG. 4. The SNR of 15 detected signals under the Smooth PSD condition and their deviations in two PSD cases. The chirp mass of the signals is indicated by color.

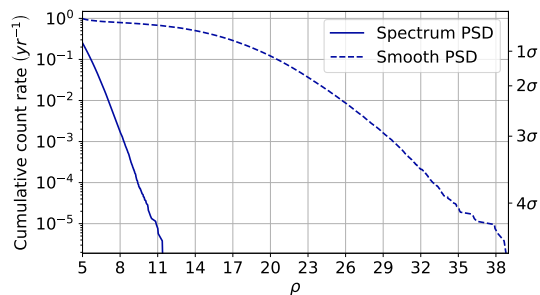


FIG. 5. The SNR distribution of false alarms, similar with Fig. 2(b), but for Sangria dataset with two kinds of PSD.

4.62 σ .

The distribution of false alarms provides interesting insights. As shown in Fig. 6, which illustrates the false alarm distribution in both scenarios, the mass-distance distribution of false alarms under the Spectrum PSD closely resembles that of LISA Gaussian noise with foreground in Fig. 3. This shows that the Spectrum PSD effectively suppresses the impact of high SNR GBs on MBHB significance. In contrast, the Smooth PSD results in significantly more false alarms with chirp masses of $10^5 \sim 10^6 M_\odot$.

Furthermore, Fig. 6 indicates that false alarms are not expected to be linked with nearby events ($\lesssim 50$ Gpc) in the mass range of $10^5 \sim 10^7 M_\odot$. Therefore, MBHB candidates detected in this range are expected to be associated with higher significance, and it is possible to use this information to further boost their significance, so that even relatively weak signals could be unambiguously identified.

For the LDC-2a dataset with an SNR threshold of 5, under the Spectrum PSD condition, the analysis required about 198 hours using 336 cores across 6 Intel Xeon Gold 6330 CPUs, while the Smooth PSD condition consumed about 328 hours due to increased false alarms. Our program is highly parallel and can utilize more cores

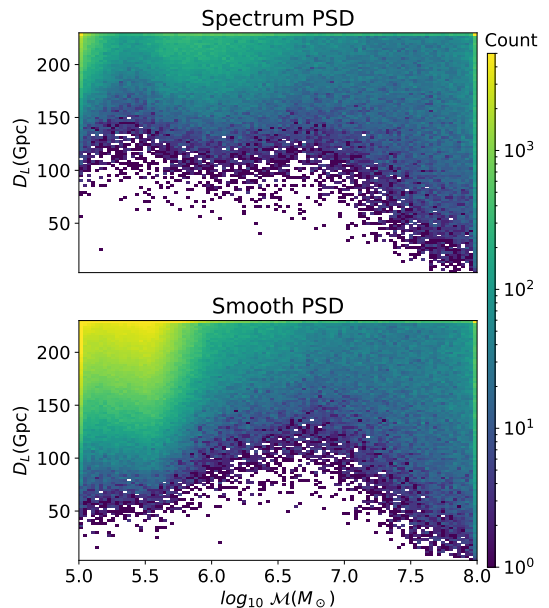


FIG. 6. The histograms of the distribution of false alarms, similar with Fig. 3, but for Sangria dataset and the SNR threshold is 5.

to achieve reduced computation time.

TABLE III. The SNR required for MBHBs to reach a specified significance level, similar with Table II, but under LDC-2a Sangria dataset with two kinds of PSDs.

	$\rho_0^{3\sigma}$	$\rho_0^{4\sigma}$
Spectrum PSD	8.15	10.09
Smooth PSD	29.32	34.64

IV. SUMMARY

Evaluating significance is essential to establish faith in future milli-Hertz GW detections. Yet, studies on implementing significance estimation algorithms are still inadequate. In this work, we develop a fast, robust, and accurate significance evaluation algorithm for MBHB mergers with space-based GW detectors. We leverage the time-shift method and the iterative Nelder-Mead algorithm, combined with the A , E , and T channel characteristics of space-based detectors, to achieve significance evaluation for MBHBs under both ideal conditions and multi-source confusion scenarios.

We applied our significance evaluation pipeline to simulated Gaussian noise data and the LDC-2a dataset, and analyzed how factors like foreground noise and GB signals affect the significance of MBHBs. For the LDC-2a dataset with multi-source confusion, we found that treating high SNR GBs as spikes in the PSD can greatly mitigate their contamination in false alarms, so that the

significance of actual MBHBs can be greatly enhanced. Our analysis of one month of Gaussian and stationary data takes several thousand core hours, whereas analyzing a year of LDC-2a data requires tens of thousands of core hours. However, given the code's high parallelizability, the actual wall-clock time remains manageable in a multi-core parallel computing environment.

In simulated Gaussian noise data, the significance of MBHB systems with SNR about 7(8) on TianQin or LISA can reach 3σ (4σ). False alarms are mostly uniformly distributed across parameters but exhibit patterns in chirp mass and luminosity distance. Fewer false alarms occur in detector-sensitive frequency bands, and they tend to cluster at the greatest distances. In addition, we have taken into account the potential impact of foreground noise on LISA. Furthermore, we considered the potential impact of foreground noise on LISA. Specifically, around 1 mHz of foreground noise, LISA's simulated Gaussian noise data generated numerous false alarms with chirp masses of $10^6 M_\odot$.

In the LDC-2a dataset, we analyzed the exclusive background using two different PSDs. Among the 15 detected MBHB sources, the maximum deviation caused by the two PSDs was only approximately 10%. However, the Spectrum PSD can significantly reduce the signal's FAR by several orders of magnitude, lowering the required SNR for a 4σ detection from around 35 to about 10. The Spectrum PSD effectively suppressed false alarms with chirp masses of $10^5 \sim 10^6 M_\odot$, which aligns with the main frequency band of the GB signals. Consequently, under the Spectrum PSD, the relationship between significance and SNR, as well as the distribution of false alarms, resembles that of Gaussian noise data with foreground noise. In contrast, the Smooth PSD led to numerous GB signals being misidentified as MBHBs, significantly increasing the FAR. Nevertheless, due to the relatively high SNR of MBHBs, in both cases, no false alarm SNR exceeded that of the detected signals. Thus, all 15 detected signals achieved a significance level exceeding 4.62σ .

Our current algorithm struggles to achieve 5σ significance, unless given longer observation times or smaller time-shift intervals. The analysis is also based on the assumption that noise PSD is given or at least uncorrelated. We plan to address these limitations in future work [51]. Enhancement is feasible, and we hereby propose several potential approaches to resolve this issue. First, capitalizing on the unique properties of MBHB signals, such as the SNR accumulation patterns [52] and the mass-distance relationship, can further refine the filtering process. This approach eliminates potential false alarms and boosts the significance of candidates matching these features. Second, future multi-detector network will exponentially increase time-shift combinations via more observational channels, enabling a longer equivalent background data construction and lower FAP limit. Third, using a Poisson estimation method, we can extrapolate and estimate the significance of higher SNR signals based

on the existing significance-SNR relationship.

ACKNOWLEDGMENT

This work has been supported by the National Key Research and Development Program of China (No. 2023YFC2206701), the Natural Science Foundation of China (Grants No. 12173104, No. 12261131504), and the science research grants from the China Manned Space Project (CMS-CSST-2025-A13). We would like to thank Jian-Dong Zhang, Han Wang and Yu-Xin Yang for helpful comments.

Appendix A: Detectors

In the 2030s, there will be many space-based GW detectors in operation, such as LISA[10] from Europe, TianQin[9] and Taiji[11] from China. These detectors all use an equilateral triangular configuration, emitting and receiving laser beams to each other, and searching GWs by detecting tiny changes in the distances between the satellites.

The TianQin detector is in a geocentric orbit and, due to its shorter arm length, is sensitive to signals in the frequency range of $10^{-4} \sim 1$ Hz. In contrast, LISA and Taiji are heliocentric orbit detectors, located 20° ahead and behind Earth's orbit, and sensitive to signals in the frequency range of $10^{-5} \sim 10^{-1}$ Hz.

Appendix B: Waveform

In this work, we utilized the IMRPhenomD template [53–55] and time delay interferometry (TDI) response [30–32] to generate MBHB signals.

The IMRPhenomD waveform is a model used in GW astronomy to describe the signal emitted by merging compact binary systems. It covers the three main stages of the merger process: inspiral, merger, and ringdown. This model is widely used in the analysis of GW data to estimate the properties of the sources and to test the predictions of general relativity. In this work, we constrained the chirp mass range of MBHBs to be between $10^5 \sim 10^8 M_\odot$, and the luminosity distance to be less than 230 Gpc, which roughly corresponds to a redshift of 20.

The TDI response describes how the detector's output signal is generated in response to the incident GW signal after applying the TDI technique. TDI is used to reduce the effects of laser frequency noise and other instrumental noises by combining the data from multiple laser links between the spacecraft with appropriate time delays. Through a simple linear combination, as shown in Equation B1, the symmetric TDI channels X , Y , Z can be transformed into the noise-uncorrelated A , E , T

channels.

$$A = \frac{1}{\sqrt{2}} (Z - X), \quad (\text{B1a})$$

$$E = \frac{1}{\sqrt{6}} (X - 2Y + Z), \quad (\text{B1b})$$

$$T = \frac{1}{\sqrt{3}} (X + Y + Z), \quad (\text{B1c})$$

Notably, the T channel is insensitive to both signal and noise at low frequencies.

-
- [1] L. Lyons, Discovering the Significance of 5 sigma, arXiv e-prints, arXiv:1310.1284 (2013), arXiv:1310.1284 [physics.data-an].
- [2] B. P. Abbott, et al (LIGO Scientific Collaboration, and V. Collaboration), GWTC-1: A Gravitational-Wave Transient Catalog of Compact Binary Mergers Observed by LIGO and Virgo during the First and Second Observing Runs, Physical Review X **9**, 031040 (2019), arXiv:1811.12907 [astro-ph.HE].
- [3] R. Abbott, et al (LIGO Scientific Collaboration, and V. Collaboration), GWTC-2: Compact Binary Coalescences Observed by LIGO and Virgo during the First Half of the Third Observing Run, Physical Review X **11**, 021053 (2021), arXiv:2010.14527 [gr-qc].
- [4] R. Abbott *et al.* (KAGRA, VIRGO, LIGO Scientific), GWTC-3: Compact Binary Coalescences Observed by LIGO and Virgo during the Second Part of the Third Observing Run, Phys. Rev. X **13**, 041039 (2023), arXiv:2111.03606 [gr-qc].
- [5] G. Agazie *et al.* (NANOGrav), The NANOGrav 15 yr Data Set: Evidence for a Gravitational-wave Background, Astrophys. J. Lett. **951**, L8 (2023), arXiv:2306.16213 [astro-ph.HE].
- [6] J. Antoniadis *et al.* (EPTA, InPTA:), The second data release from the European Pulsar Timing Array - III. Search for gravitational wave signals, Astron. Astrophys. **678**, A50 (2023), arXiv:2306.16214 [astro-ph.HE].
- [7] D. J. Reardon *et al.*, Search for an Isotropic Gravitational-wave Background with the Parkes Pulsar Timing Array, Astrophys. J. Lett. **951**, L6 (2023), arXiv:2306.16215 [astro-ph.HE].
- [8] H. Xu *et al.*, Searching for the Nano-Hertz Stochastic Gravitational Wave Background with the Chinese Pulsar Timing Array Data Release I, Res. Astron. Astrophys. **23**, 075024 (2023), arXiv:2306.16216 [astro-ph.HE].
- [9] J. Luo *et al.* (TianQin), TianQin: a space-borne gravitational wave detector, Class. Quant. Grav. **33**, 035010 (2016), arXiv:1512.02076 [astro-ph.IM].
- [10] P. Amaro-Seoane *et al.* (LISA), Laser Interferometer Space Antenna, arXiv e-prints, arXiv:1702.00786 (2017), arXiv:1702.00786 [astro-ph.IM].
- [11] W.-R. Hu and Y.-L. Wu, The Taiji Program in Space for gravitational wave physics and the nature of gravity, Natl. Sci. Rev. **4**, 685 (2017).
- [12] Y. Gong, J. Luo, and B. Wang, Concepts and status of Chinese space gravitational wave detection projects, Nature Astron. **5**, 881 (2021), arXiv:2109.07442 [astro-ph.IM].
- [13] H.-T. Wang *et al.*, Science with the TianQin observatory: Preliminary results on massive black hole binaries, Phys. Rev. D **100**, 043003 (2019), arXiv:1902.04423 [astro-ph.HE].
- [14] M. L. Katz and S. L. Larson, Evaluating Black Hole Detectability with LISA, Mon. Not. Roy. Astron. Soc. **483**, 3108 (2019), arXiv:1807.02511 [gr-qc].
- [15] E. Berti, A. Buonanno, and C. M. Will, Estimating spinning binary parameters and testing alternative theories of gravity with LISA, Phys. Rev. D **71**, 084025 (2005), arXiv:gr-qc/0411129.
- [16] E. Berti, A. Buonanno, and C. M. Will, Testing general relativity and probing the merger history of massive black holes with LISA, Class. Quant. Grav. **22**, S943 (2005), arXiv:gr-qc/0504017.
- [17] J. R. Gair, M. Vallisneri, S. L. Larson, and J. G. Baker, Testing General Relativity with Low-Frequency, Space-Based Gravitational-Wave Detectors, Living Rev. Rel. **16**, 7 (2013), arXiv:1212.5575 [gr-qc].
- [18] K. Yagi and L. C. Stein, Black Hole Based Tests of General Relativity, Class. Quant. Grav. **33**, 054001 (2016), arXiv:1602.02413 [gr-qc].
- [19] A. Sesana, M. Volonteri, and F. Haardt, The imprint of massive black hole formation models on the LISA data stream, Mon. Not. Roy. Astron. Soc. **377**, 1711 (2007), arXiv:astro-ph/0701556.
- [20] K. Inayoshi, E. Visbal, and Z. Haiman, The Assembly of the First Massive Black Holes, Ann. Rev. Astron. Astrophys. **58**, 27 (2020), arXiv:1911.05791 [astro-ph.GA].
- [21] B. F. Schutz, Determining the Hubble Constant from Gravitational Wave Observations, Nature **323**, 310 (1986).
- [22] S. A. Hughes, Untangling the merger history of massive black holes with LISA, Mon. Not. Roy. Astron. Soc. **331**, 805 (2002), arXiv:astro-ph/0108483.
- [23] N. Tamanini, C. Caprini, E. Barausse, A. Sesana, A. Klein, and A. Petiteau, Science with the space-based interferometer eLISA. III: Probing the expansion of the Universe using gravitational wave standard sirens, JCAP **2016** (4), 002, arXiv:1601.07112 [astro-ph.CO].
- [24] L.-G. Zhu, Y.-M. Hu, H.-T. Wang, J.-d. Zhang, X.-D. Li, M. Hendry, and J. Mei, Constraining the cosmological parameters using gravitational wave observations of massive black hole binaries and statistical redshift information, Phys. Rev. Res. **4**, 013247 (2022), arXiv:2104.11956 [astro-ph.CO].

- [25] S. Babak *et al.*, Searching for gravitational waves from binary coalescence, *Phys. Rev. D* **87**, 024033 (2013), arXiv:1208.3491 [gr-qc].
- [26] K. Cannon, C. Hanna, and D. Keppel, Method to estimate the significance of coincident gravitational-wave observations from compact binary coalescence, *Phys. Rev. D* **88**, 024025 (2013), arXiv:1209.0718 [gr-qc].
- [27] P. L. Bender and D. Hils, Confusion noise level due to galactic and extragalactic binaries, *Class. Quant. Grav.* **14**, 1439 (1997).
- [28] T. Robson and N. Cornish, Impact of galactic foreground characterization on a global analysis for the LISA gravitational wave observatory, *Class. Quant. Grav.* **34**, 244002 (2017), arXiv:1705.09421 [gr-qc].
- [29] T. B. Littenberg and N. J. Cornish, Prototype global analysis of LISA data with multiple source types, *Phys. Rev. D* **107**, 063004 (2023), arXiv:2301.03673 [gr-qc].
- [30] M. Vallisneri, Synthetic LISA: Simulating time delay interferometry in a model LISA, *Phys. Rev. D* **71**, 022001 (2005), arXiv:gr-qc/0407102.
- [31] S. Marsat, J. G. Baker, and T. Dal Canton, Exploring the Bayesian parameter estimation of binary black holes with LISA, *Phys. Rev. D* **103**, 083011 (2021), arXiv:2003.00357 [gr-qc].
- [32] E.-K. Li *et al.*, GWSpace: a multi-mission science data simulator for space-based gravitational wave detection, arXiv e-prints , arXiv:2309.15020 (2023), arXiv:2309.15020 [gr-qc].
- [33] C. Pitte, Q. Baghi, S. Marsat, M. Besançon, and A. Petiteau, Detectability of higher harmonics with LISA, *Phys. Rev. D* **108**, 044053 (2023), arXiv:2304.03142 [gr-qc].
- [34] N. J. Cornish, Low latency detection of massive black hole binaries, *Phys. Rev. D* **105**, 044007 (2022), arXiv:2110.06238 [gr-qc].
- [35] S. Deng, S. Babak, M. Le Jeune, S. Marsat, É. Plagnol, and A. Sartirana, Modular global-fit pipeline for LISA data analysis, arXiv e-prints , arXiv:2501.10277 (2025), arXiv:2501.10277 [gr-qc].
- [36] S. H. Strub, L. Ferraioli, C. Schmeltz, S. C. Stähler, and D. Giardini, Global analysis of LISA data with Galactic binaries and massive black hole binaries, *Phys. Rev. D* **110**, 024005 (2024), arXiv:2403.15318 [gr-qc].
- [37] T. Littenberg, N. Cornish, K. Lackeos, and T. Robson, Global Analysis of the Gravitational Wave Signal from Galactic Binaries, *Phys. Rev. D* **101**, 123021 (2020), arXiv:2004.08464 [gr-qc].
- [38] M. L. Katz, N. Karnesis, N. Korsakova, J. R. Gair, and N. Stergioulas, Efficient GPU-accelerated multisource global fit pipeline for LISA data analysis, *Phys. Rev. D* **111**, 024060 (2025), arXiv:2405.04690 [gr-qc].
- [39] H.-Y. Chen, X.-Y. Lyu, E.-K. Li, and Y.-M. Hu, Near real-time gravitational wave data analysis of the massive black hole binary with TianQin, *Sci. China Phys. Mech. Astron.* **67**, 279512 (2024), arXiv:2309.06910 [gr-qc].
- [40] <https://lisa-ldc.lal.in2p3.fr/challenge2a>.
- [41] G. S. Davies, T. Dent, M. Tápai, I. Harry, C. McIsaac, and A. H. Nitz, Extending the PyCBC search for gravitational waves from compact binary mergers to a global network, *Phys. Rev. D* **102**, 022004 (2020), arXiv:2002.08291 [astro-ph.HE].
- [42] B. P. Abbott *et al.* (LIGO Scientific, Virgo), Binary Black Hole Mergers in the first Advanced LIGO Observing Run, *Phys. Rev. X* **6**, 041015 (2016), [Erratum: *Phys. Rev. X* **8**, 039903 (2018)], arXiv:1606.04856 [gr-qc].
- [43] C. Capano, T. Dent, C. Hanna, M. Hendry, Y.-M. Hu, C. Messenger, and J. Veitch, Systematic errors in estimation of gravitational-wave candidate significance, *Phys. Rev. D* **96**, 082002 (2017), arXiv:1708.06710 [astro-ph.IM].
- [44] N. J. Cornish and E. K. Porter, Catching supermassive black hole binaries without a net, *Phys. Rev. D* **75**, 021301 (2007), arXiv:gr-qc/0605135.
- [45] C. J. Moore, D. Gerosa, and A. Klein, Are stellar-mass black-hole binaries too quiet for LISA?, *Mon. Not. Roy. Astron. Soc.* **488**, L94 (2019), arXiv:1905.11998 [astro-ph.HE].
- [46] J. A. Nelder and R. Mead, A Simplex Method for Function Minimization, *Comput. J.* **7**, 308 (1965).
- [47] J. C. Lagarias, J. A. Reeds, M. H. Wright, and P. E. Wright, Convergence Properties of the Nelder-Mead Simplex Method in Low Dimensions, *SIAM J. Optim.* **9**, 112 (1998).
- [48] S. Singer and S. Singer, Efficient implementation of the nelder-meade search algorithm, *Applied Numerical Analysis & Computational Mathematics* **1**, 524 (2004).
- [49] R. Balasubramanian, B. S. Sathyaprakash, and S. V. Dhurandhar, Gravitational waves from coalescing binaries: Detection strategies and Monte Carlo estimation of parameters, *Phys. Rev. D* **53**, 3033 (1996), [Erratum: *Phys. Rev. D* **54**, 1860 (1996)], arXiv:gr-qc/9508011.
- [50] T. A. Prince, M. Tinto, S. L. Larson, and J. W. Armstrong, The LISA optimal sensitivity, *Phys. Rev. D* **66**, 122002 (2002), arXiv:gr-qc/0209039.
- [51] Y.-N. Li, Y.-M. Hu, and E.-K. Li, Adaptive Modeling of Correlated Noise in Space-Based Gravitational Wave Detectors, arXiv e-prints , arXiv:2504.12983 (2025), arXiv:2504.12983 [astro-ph.IM].
- [52] H.-Y. Chen, H. Wang, E.-K. Li, and Y.-M. Hu, Signal-to-noise Ratio Analytic Formulae of the Inspirational Binary Black Holes in TianQin, arXiv e-prints , arXiv:2410.19401 (2024), arXiv:2410.19401 [astro-ph.GA].
- [53] S. Husa, S. Khan, M. Hannam, M. Pürrer, F. Ohme, X. Jiménez Forteza, and A. Bohé, Frequency-domain gravitational waves from nonprecessing black-hole binaries. I. New numerical waveforms and anatomy of the signal, *Phys. Rev. D* **93**, 044006 (2016), arXiv:1508.07250 [gr-qc].
- [54] S. Khan, S. Husa, M. Hannam, F. Ohme, M. Pürrer, X. Jiménez Forteza, and A. Bohé, Frequency-domain gravitational waves from nonprecessing black-hole binaries. II. A phenomenological model for the advanced detector era, *Phys. Rev. D* **93**, 044007 (2016), arXiv:1508.07253 [gr-qc].
- [55] M. C. Digman and N. J. Cornish, Parameter estimation for stellar-origin black hole mergers in LISA, *Phys. Rev. D* **108**, 023022 (2023), arXiv:2212.04600 [gr-qc].